3D Localization and Mapping using mm-Wave: What are the Opportunities in Vehicular and Indoor Environments?

Ali Yassin*, Youssef Nasser*, Yoann Corre†, Gregory Gougeon†, Yves Lostanlen†

* American University of Beirut, Beirut, Lebanon 1107 2020, ahy04@mail.aub.edu
† Siradel, Parc de Brocéliande 35760 Saint Grégoire, France, ycorre@siradel.com

***Abstract*—This paper raises an important question on the opportunities offered by millimeter Waves (mmWaves) signals for 3D localization and mapping (3D-LOCMAP) in vehicular and indoor environments. More precisely, the paper presents a technical framework for 3DLOCMAP using the mmWave channel response and mmWave propagation characteristics. To do so, the paper firstly introduces a combination between Triangulateration (TL) and Received Signal Strength (RSS) or Time of Arrival (ToA) measurements for 3DLOCMAP. In the case of a channel model with single bounce, the environment mapping (such as obstacles) is achieved by estimating the positions of virtual anchor nodes (VANs), known as mirrors of the real anchors with respect to obstacle. Then, the obstacle position and dimensions are found via the estimation of the reflector points on the obstacle. In case of double-bounce, the scenario is observed from single-bounce perspective by estimating Virtual Receiver (VRx), VAN, and two Points of Reflection (PoR). Simulation results have shown the accuracy of the proposed framework which can be extended for further investigations. The work here will open the door for multiple applications in vehicular, robotics, health, radar-like systems, and Internet of Things (IoT).**

***Index Terms*—Millimeter wave, Localization, Mapping, Context Inference, Virtual Anchor Node (VAN), Obstacle Detection and Classification.**

I. Introduction

Localization approaches have grown in the last decade offering a wide range of localization services targeting different applications: health, environment, indoor coverage, etc. These approaches are based on different radio technologies such WiFi access points, Ultra-Wide Bands (UWB), and dead reckoning. Non-radio technologies have been also proposed in literature based mostly on cameras at the expense of additional cost, equipment and privacy issues. On the other side, milliMeter Wave (mmWave) wireless communication systems have recently gained great research interests due to their benefits in terms of spectrum, propagation characteristics, potential applications and services [1]. Applications based on multi gigabit data rates are increasing in demands. Hence, mmWave is evolving due to the availability of a large bandwidth. Technically, mmWave spectrum ranges between 30 GHz and 300 GHz and can be used for military, radar and cellular services. For instance, the spectrum at 28 GHz, 38 GHz, and 70-80 GHz provides promising channel propagation specifications for the evolving fifth generation (5G) of cellular systems [2][3]. The indoor networking of 5G mobile wireless communication is based on 60 GHz technology that is embracing the small cell deployment. The shortness of the coverage range at mmWave frequencies triggers the deployment of a capillary network of Access Points (APs) in the buildings offering enhancements in terms of localization. Among the potential services offered by mmWave, localization and mapping appear as key factors in enabling new means and tools for communications systems [6]. Recently, researchers have also looked at mmWave application in vehicular networks and autonomous cars [4][5]. Indeed, the use of mmWave bands offers very large data rates and allows the cars to exchange raw data. Moreover, in autonomous cars, the sensors can exploit these rates more efficiently. The application of mmWave in vehicular can be also used for cars positioning and tracking, accident avoidance and obstacle detection (environment mapping). In terms of channel propagation, the different research works have shown that mmWave propagation channel holds different characteristics from Snell's Law.

Indeed, at mmWave the channel Line-of-Sight (LoS) path is assumed to be dominant, i.e. the propagation at these frequencies is considered quasi-optical [7], while the Non-Line-of-Sight (NLoS) component fades drastically after one or two reflections. Hence, mmWave channel models take into consideration no more than single-bounce reflection effect [8]. Moreover, it has been shown that the scattering effect is very low at these frequencies which makes the communications between nodes very critical in NLoS situations [9]. Hence, the transmitted beam will have the same directivity after reflections with slight scattering[10]. From localization perspective, as Snell's law holds at mmWave, i.e. the equality between the angles of departure and incidence upon reflection [11], and scattering is very limited, it is very challenging to propose technologies and approaches offering high accuracy. Nevertheless, if these characteristics are considered, localization procedures and mapping approaches can be derived [3][12]-[19].

In literature, there exist few researches on localization systems operating at 60 GHz. Most of the research work done focused on measuring the delay spread used for systems based on Time of Arrival (ToA), Time Difference of Arrival (TDoA) and Angle of Arrival (AoA) methods [14][15]. In this paper, we tackle the joint problem of 3D localization and mapping (3DLOCMAP). The high-level proposed approach is shown in Figure 1. It allows us developing context inference and mapping of the environment with high accuracy reaching sub meters (few centimeters in some cases). In this work, we are tackling two different environments: the vehicular and indoor and we propose a framework for 3DLOCMAP using a professional mmWave channel simulator. The contribution of the paper can be summarized in the following aspects:

- Exploitation of the map-based mmWave channel criteria

978-1-5386-2321-3/18/$31.00 ©2018 IEEE

to provide 3D localization and mapping. MmWave signals have no scattering effect and they realize high penetration loss through obstacles. This fact triggers the use of Snell's law for obstacle detection and classification.

- We use the concept of Virtual Anchor Nodes (VANs) to estimate the location of each mmWave receiver (Rx) using the combination between the proposed Triangulateration (TL) technique and RSS or ToA.
- Introduction of the virtual receiver (VRx) to develop environment mapping in the case of double-bounce channel propagation
- Validation of proposed approaches through extensive simulation results.

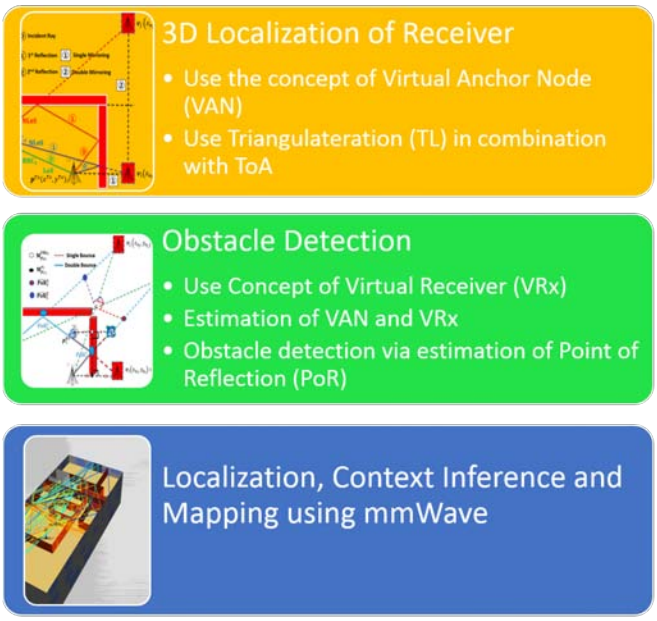

Fig. 1. The process of localization, context inference and mapping using geometric approach

The rest of this paper is organized as follows. In Section 2, we develop the system model and the 3D localization methodology of the receiver using mmWave. In Section 3, we propose new approaches for context inference by estimating obstacles positions, size and type. In Section 4, we provide simulation results while conclusions are drawn in Section 5.

II. System Model using Millimeter Wave

A. Environment Settings

The proposed mmWave localization techniques are tested in a 3D environment. The boundaries and radio-reflective obstacles in the reflective objects are grouped in a set O. Obstacles are described as three-dimensional flat polygonal faces with sharp vertices and straight edges. Each oriented surface S of 3D obstacle is denoted by its perpendicular line, written as:

$$a(x - p_x) + b(y - p_y) + c(z - p_z) + d = 0 \quad (1)$$

where $\mathbf{p} = \left(p_x, p_y, p_z\right)$ is a point of intersection between the surface and its perpendicular and $\vec{n} = (a, b, c)$ is the vector orthogonal to the surface S. By assumption, a single mmWave AP is deployed at a location $\mathbf{p}^{Tx}$. Additionally, the AP is assumed to broadcast its position and the specifications of the objects in O to the node(s) targeted for localization. In this paper, the AoA will be firstly prioritized and investigated since the AoA metric is not sensitive to the absorption loss at mmWave. It will be then complemented by other metrics, such as RSS and ToA, when necessary. The AoA spectrum, $P_p(\theta)$, is a $3 \times N_p$ matrix that records the amplitude of each received ray component (RRC) as a function of the azimuth θ and elevation ϕ at a given location $\mathbf{p}$, where N_p is the number of RRCs. Each RRC can be either due to a LoS link between the transmitter and the receiver or due to NLoS link induced by reflections of one or more surfaces in the obstacle set O. Then, $SP_p(\theta)$ is a $3 \times N_p$ matrix, which contains in its first row the amplitude of each RRC sorted in decreasing order, in its second row the azimuth θ with respect to reference angle θ_0, and in its third row the elevation ϕ with respect to reference angle ϕ_0. Moreover, the boundaries of the testing environment are assumed to be known for the node(s) to be localized.

B. Virtual Anchors

As the environment is unknown, the NLoS rays are recognized as virtual LoS rays transmitted from VANs to fulfill the condition on the number of anchor nodes needed for localization. The first column vector of $SP_p(\theta, \phi)$ represents the LoS path between the transmitter and the receiver to be localized, and the columns $2 : N_p$ represent the NLoS paths. So, we have $N_p - 1$ RRCs that correspond to NLoS paths. Each of these paths can be modeled as emitted by a VAN through a virtual LoS path reaching the receiver $\mathbf{p}^{Rx}$. The locations of the VANs are determined by mirroring the AP $\mathbf{p}^{Tx}$ with respect to the surfaces in the obstacle set O since it is the source of signal reflections. We denote $V = \{v_0, v_1, \ldots\}$ to be the set of the positions of all possible VANs, and we denote $\overline{V} = \{V_0, V_1, \ldots\}$ to be a partition of V. We let $V_0 = \mathbf{p}^{Tx}$, and each set $V_i, i = 1, 2, \ldots$ represents all VANs that have been mirrored i times due to reflections caused by any surface in the obstacle set O. Actually, there is no limit on the number of reflections of the signal transmitted by $\mathbf{p}^{Tx}$. However, a mmWave signal fades quickly during its propagation as it reflects off the surfaces. So, we limited the set V by assuming a maximum reflection order $\mu = 2$. Hence, the set of all VANs will be represented as $V_\mu = \bigcup_{i=0}^{\mu} V_i$. As shown in Figure 2, the anchors $v_i \in V_1$ represent first order of reflection and the anchors $v_i \in V_2$ represent second order of reflection.

III. Localization of the Receiver in an unknown environment: The Proposed Algorithm

As the environment is assumed to be unknown in this section, i.e. none of the $\mathbf{v}_i$ is known except the true TX position $\mathbf{v}_0$, the first step in the localization and mapping consists in finding the positions of the receiver and of the VANs and of the VRx. To solve this problem, we can easily assume that there are enough measurements about ToA/RSS/AoA[1]. The proposed algorithm is divided into two main steps: (1) filtering the received signal and (2) localization through hybrid approach

[1]this assumption is valid and solid as these measurements are needed for channel estimation at mmWave

A. Filtering the Received Rays

In a dense environment, such as indoor or dense vehicular environment, many of the rays will be received after few reflections. Hence, their powers will be beneath the noise power. In order to reduce the localization error and avoid the noise effect on the received rays' powers, the first step in the proposed algorithm is to filter out the signal keeping the strong rays. To do so, the rays are first sorted based on ToA values in ascending order where the first ray is the ray received with minimum delay. Then knowing that the noise variance is equal to $-174 + 10 \times \log_{10}(BW)$, the signal is filtered out to keep the strongest rays based on a received power threshold, γ_{P^r}, calculated as follows:

$$\gamma_{P^r} = -174 + 10 \times \log_{10}(BW) + 10 \times \log_{10}\left(\frac{1 + Q^{-1}(PFA)}{\sqrt{N_p}}\right) \quad (2)$$

where BW is the bandwidth, $Q^{-1}(.)$ is the inverse Q function, and PFA is the probability of false alarm to separate a ray (with a given delay) from noise.

B. Estimating the Rx Position

The estimation of the Rx position is done by appropriate combination of the channel metrics. Without loss of generality, let us assume that the first received path corresponds to a LoS. Hence, we can easily write (see Fig. 2):

$$\begin{cases} x^{Rx} = x^{Tx} + \rho_0 \sin\left(\phi_0^{AoA}\right) \cos\left(\theta_0^{AoA}\right) \\ y^{Rx} = y^{Tx} + \rho_0 \sin\left(\phi_0^{AoA}\right) \sin\left(\theta_0^{AoA}\right) \\ z^{Rx} = z^{Tx} + \rho_0 \cos\left(\phi_0^{AoA}\right) \end{cases} \quad (3)$$

where $\mathbf{p}^{Tx} = \left(x^{Tx}, y^{Tx}, z^{Tx}\right)$, $\mathbf{p}^{Rx} = \left(x^{Rx}, y^{Rx}, z^{Rx}\right)$, ρ_0 is the distance traveled by the first ray, and ϕ_0^{AoA} and θ_0^{AoA} are the elevation and the azimuth of the AoA for the ray assumed to be in LoS. Consequently, the estimated receiver position $\hat{\mathbf{p}}^{Rx}$ is calculated as follows:

$$\hat{\mathbf{p}}^{Rx} = \mathbf{p}^{Tx} + \rho_0 \begin{bmatrix} \sin\left(\phi_0^{AoA}\right) \cos\left(\theta_0^{AoA}\right) \\ \sin\left(\phi_0^{AoA}\right) \sin\left(\theta_0^{AoA}\right) \\ \cos\left(\phi_0^{AoA}\right) \end{bmatrix} \quad (4)$$

It is very clear from (4) that the estimation of the Rx position requires the knowledge of the distance ρ_0 traveled by the LoS path. The latter could be easily estimated using either RSS or ToA metric as follows.

1) RSS: RSS is used to estimate the distance traveled by each ray using the free space pathloss model. The pathloss for each ray is calculated first as follows:

$$PL_i = P^t - P_i^r - 20 \times \log_{10}\left(\frac{4 \times \pi \times f_c}{c}\right) \quad (5)$$

where PL_i is the pathloss for the ith path, c is the speed of light, P^t is the transmitted power in dB, P_i^r is the received power for the ith path in dB and f_c is the carrier frequency. Thus, the distance traveled by the ith ray is then estimated as follows:

$$\rho_i = 10^{PL_i/20} \quad (6)$$

2) ToA: ToA can also be used to estimate the distance traveled by each ray as follows:

$$\rho_i = c \times toa_i \quad (7)$$

where toa_i is the ToA for the ith ray.

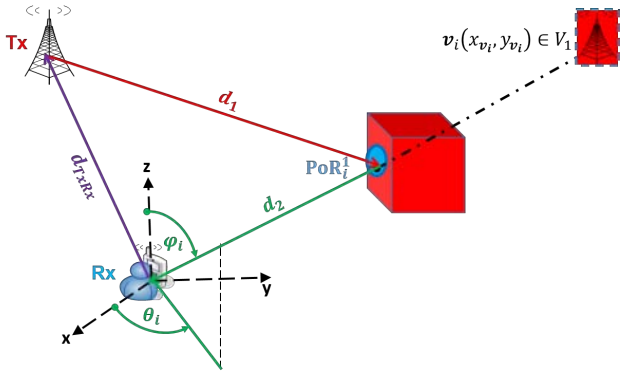

Fig. 2. VANs related to first order of reflection

Hence, using ρ_0 from (6) or (7) in (4), the estimation of the Rx position in an unknown environment can be directly obtained.

IV. Obstacle Mapping in Single Bounce Scenario

The main target of this section is to estimate obstacles locations and their dimensions using the received signal. We introduce obstacle detection in three steps; (1) estimate the position of the VANs, (2) estimate the positions of VRx, and (3) estimate the obstacle direction and dimensions by finding the points of reflection on the obstacles, as shown in 3. The VANs and the receiver are estimated using the TL algorithm for NLoS environments. Then, we will use the concept of mirroring to detect the obstacle in between the transmitter and the VANs.

A. Estimation of the VAN Positions

The model in (6) can be easily extended to NLoS rays for obstacle mapping. Here, two different scenarios can be targeted: single bounce and double bounce.

1) Single Bounce Scenario: After estimating the Rx position, we need to estimate the VANs for rays coming from NLoS paths. In case of single bounce scenario, the paths are considered to be transmitted from virtual transmitters denoted by VANs. In other words, the received ray coming through NLoS path is considered to be a virtual LoS path coming from the VAN. The VANs are estimated for the 3D geometric model shown in Figure 2 as follows:

$$\begin{cases} x_i^v = x^{Rx} + \rho_i \sin\left(\phi_i^{AoA}\right) \cos\left(\theta_i^{AoA}\right) \\ y_i^v = y^{Rx} + \rho_i \sin\left(\phi_i^{AoA}\right) \sin\left(\theta_i^{AoA}\right) \\ z_i^v = z^{Rx} + \rho_i \cos\left(\phi_i^{AoA}\right) \end{cases} \quad (8)$$

where $\mathbf{v}_i = \left(x_i^v, y_i^v, z_i^v\right)$ is the VAN corresponding to the i-th NLoS ray where $i = 1, \cdots, N_p - 1$ and ρ_i is the distance traveled by the corresponding path.

B. Obstacle Detection through Points of Reflection

After estimating the VANs, we need to categorize them into two sets: The first one is the set of VANs that are obtained due to walls, floor and ceiling reflections, and the second one is the set of VANs that are obtained due to obstacle reflections. This classification can be done by applying the concept of mirroring over the transmitter with respect to the room boundaries in order to find the VANs of the first set. Hence, we will be able to identify the VANs that are due to obstacle reflections. The obstacle is detected by estimating the points of reflection, gathered as cloud of reflection points (CoRP) of the rays induced by the obstacle. If the size of this CoRP is large enough, a good estimation by interpolation and extrapolation of the obstacle sides (hence obstacle shape) is possible. However, for a given receiver position and a single transmitter, the set of VANs and hence the size of the CoRP is limited leading to a biased estimation of the obstacle shape. Hence, we need to increase the number of APs in order to estimate all the VANs required to do perfect estimation of the obstacle.

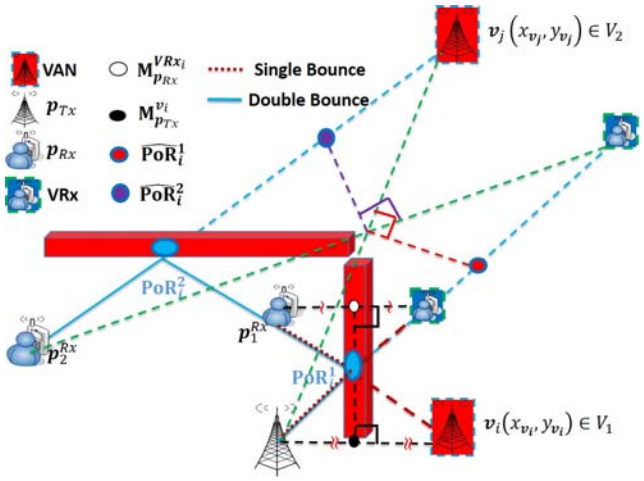

Fig. 3. VAN and VRx related to first and second order of reflection

The estimation of the reflection point could be done in different ways, depending on the available measurements. It is mainly based on the geometry of reflected rays, obstacle orientation and the positions of VANs and Rx. In the sequel, we assume that the angle of departure (AoD) for each ray is known [2]. First, the midpoint between the transmitter and VAN $\mathbf{v}_i$ is calculated as follows:

$$\mathbf{M}_{\mathbf{p}^{Tx}}^{\mathbf{v}_i} = \frac{\mathbf{p}^{Tx} + \mathbf{v}_i}{2} \tag{9}$$

where $\mathbf{M}_{\mathbf{p}^{Tx}}^{\mathbf{v}_i} = \left(x^{\mathbf{M}_{\mathbf{p}^{Tx}}^{\mathbf{v}_i}}, y^{\mathbf{M}_{\mathbf{p}^{Tx}}^{\mathbf{v}_i}}, z^{\mathbf{M}_{\mathbf{p}^{Tx}}^{\mathbf{v}_i}}\right)$. Then, the normal to the point of reflection (PoR) $\mathbf{PoR}_1^i$ corresponding to VAN $\mathbf{v}_i$ is calculated as follows:

$$\mathbf{n}_i^{PoR_1} = \mathbf{p}^{Tx} - \mathbf{v}_i \tag{10}$$

[2]this assumption is considered here for the ease of derivations. if this information is not available the estimation can still be done at the expense of additional calculation complexity

where $\mathbf{n}_i^{PoR_1} = \left(x_{n_i^{PoR_1}}, y_{n_i^{PoR_1}}, z_{n_i^{PoR_1}}\right)$. Then, the vector crossing the PoR $\mathbf{PoR}_i^1$ from the receiver to the transmitter is represented as follows:

$$\mathbf{w}_i = \mathbf{v}_i - \mathbf{p}^{Rx} \tag{11}$$

where $\mathbf{w}_i = (x^{w_i}, y^{w_i}, z^{w_i})$. Then, we solve for the points of intersection between VANs and the receiver to estimate the PoRs as follows:

$$\mathbf{PoR}_i^1 = \mathbf{p}^{Rx} + \left(inv\left(diag\left(\mathbf{n}_i^{PoR_1}.\mathbf{w}_i\right)\right) \times \left(\left(\mathbf{M}_{\mathbf{p}^{Tx}}^{\mathbf{v}_i} - \mathbf{p}^{Rx}\right) \times \mathbf{n}_i^{PoR_1}\right)^T\right)^T .\mathbf{w}_i \tag{12}$$

Then, the distance traveled by each ray coming from NLoS path passing from the transmitter to the receiver through the PoR is estimated as follows:

$$\rho_i^{Tx-PoR-Rx} = \sqrt{\left(x^{Tx} - x_i^{PoR}\right)^2 + \left(y^{Tx} - y_i^{PoR}\right)^2 + \left(z^{Tx} - z_i^{PoR}\right)^2} + \sqrt{\left(x^{Rx} - x_i^{PoR}\right)^2 + \left(y^{Rx} - y_i^{PoR}\right)^2 + \left(z^{Rx} - z_i^{PoR}\right)^2} \tag{13}$$

C. Estimation of the Reflection Coefficient

The reflection coefficient that corresponds to the absorption loss induced by the reflection of the obstacle can be determined for each NLoS path. It is calculated using the RSS value as follows:

$$\Gamma_i = PL_i - \left(P^t - 20 \times \log_{10}\left(d_i^{travel}\right) - 20 \times \log_{10}\left(\frac{4 \times \pi \times f_c}{c}\right) + 4.3\right) \tag{14}$$

V. Obstacle Detection for double-bounce scenario

A. Estimation of the VAN and VRx Positions

As shown in Fig. 3, the double bounce scenario is observed as two stages of single bounce scenario. Here, two points of reflection are to be considered. Moreover, we introduce the virtual receiver (VRx) defined by mirroring Rx on each obstacle. In practice, VRx position is unknown and has to be estimated. It is very useful in this scenario in order to estimate the two points of reflection, as it will be detailed later. Similar to the single bounce scenario, the distance traveled by each ray is estimated using either the ToA or RSS measurements. Assuming the ray with the strongest RSS value and minimum ToA to be the LoS path, the receiver position is estimated using (4). As the Angle of Departure (AoD) of each ray is in general known through channel estimation, then VRx position is estimated as follows:

$$\begin{cases} x_i^{VRx} = x^{Tx} + \rho_i \sin\left(\phi_i^{AoD}\right)\cos\left(\theta_i^{AoD}\right) \\ y_i^{VRx} = y^{Tx} + \rho_i \sin\left(\phi_i^{AoD}\right)\sin\left(\theta_i^{AoD}\right) \\ z_i^{VRx} = z^{Tx} + \rho_i \cos\left(\phi_i^{AoD}\right) \end{cases} \tag{15}$$

where $\mathbf{p}^{VRx} = \left(x^{VRx}, y^{VRx}, z^{VRx}\right)$, and ϕ_i^{AoD} and θ_i^{AoD} are the elevation and the azimuth of the AoD for the ith ray sent by transmitter.

It is worth mentioning that, in the case of double bounce scenario, the positions of the VANs can be easily estimated

through (8). Similar to the single-bounce scenario, the set of VANs induced by obstacle reflection is determined using (15). Double-bounce scenario is observed as two steps of single bounce scenario where the first PoR is the VRx that is estimated as $\mathbf{PoR}_i^1$ is estimated in a single bounce scenario. After estimating the VRx, the second step of single-bounce is between the VRx and the transmitter in order to estimate the second PoR $\mathbf{PoR}_i^2$ shown in Figure 3.

B. Estimation of the Reflection Points

The estimation of the reflection point could be done in different ways, depending on the available measurements. It is mainly based on the geometry of reflected rays, obstacle orientation and the positions of VANs and Rx. In the sequel, we assume that the angle of departure (AoD) for each ray is known [3]. First, the midpoint between the receiver and VRx is calculated as follows:

$$\mathbf{M}_{\mathbf{p}^{Rx}}^{\mathbf{VRx}_i} = \frac{\mathbf{p}^{Rx} + \mathbf{VRx}_i}{2} \tag{16}$$

where $\mathbf{M}_{\mathbf{p}^{Rx}}^{\mathbf{VRx}_i} = \left(x^{\mathbf{M}_{\mathbf{p}^{Rx}}^{\mathbf{VRx}_i}}, y^{\mathbf{M}_{\mathbf{p}^{Rx}}^{\mathbf{VRx}_i}}, z^{\mathbf{M}_{\mathbf{p}^{Rx}}^{\mathbf{VRx}_i}}\right)$. Then, the normal to the second PoR $\mathbf{PoR}_i^2$ corresponding to VRx $\mathbf{VRx}_i$ is calculated as follows:

$$\mathbf{n}_i^{PoR_2} = \mathbf{p}^{Rx} - \mathbf{VRx}_i \tag{17}$$

where $\mathbf{n}_i^{PoR_2} = \left(x_{n_i^{PoR_2}}, yn_i^{PoR_2}, zn_i^{PoR_2}\right)$. Then, the vector crossing the PoR $\mathbf{PoR}_i^2$ from the transmitter to the VRx is represented as follows:

$$\mathbf{w}_i = \mathbf{VRx}_i - \mathbf{p}^{Tx} \tag{18}$$

where $\mathbf{w}_i = \left(x_i^w, y_i^w, z_i^w\right)$. Then, we solve for the points of intersection between VRxs and the transmitter to estimate the PoRs as follows:

$$\mathbf{PoR}_i^2 = \mathbf{p}^{Tx} + \left(inv\left(diag\left(\mathbf{n}_i^{PoR_2}.\mathbf{w}_i\right)\right) \times \left(\left(\mathbf{M}_{\mathbf{p}^{Rx}}^{\mathbf{VRx}_i} - \mathbf{p}^{Tx}\right) \times \mathbf{n}_i^{PoR_2}\right)^T\right)^T .\mathbf{w}_i \tag{19}$$

Then, the distance traveled by each ray coming from NLoS path passing from the transmitter to the receiver through the PoR is estimated using (13). The reflection coefficient is then estimated using (14).

C. Correction of the Estimated Positions of PoR

After estimating the PoR, the target is to estimate the AoD and AoA so that we compare with exact results. The estimated elevation angle of AoD, $\hat{\phi}_i^{AoD}$, is estimated as follows:

$$\hat{\phi}_i^{AoD} = -\sin^{-1}\left(\frac{z_i^{PoR_1} - z^{Tx}}{d_i^{Tx-PoR_1}}\right) \tag{20}$$

where $d_i^{Tx-PoR_1} = \sqrt{\left(x^{Tx} - x_i^{PoR_1}\right)^2 + \left(y^{Tx} - y_i^{PoR_1}\right)^2 + \left(z^{Tx} - z_i^{PoR_1}\right)^2}$ is the distance between the estimated first PoR $\mathbf{PoR}_1^i$ and the transmitter $\mathbf{p}^{Tx}$. On the other hand, the estimated elevation angle of AoA, $\hat{\phi}_i^{AoA}$, is estimated as follows:

$$\hat{\phi}_i^{AoA} = -\sin^{-1}\left(\frac{z_i^{PoR_2} - z^{Rx}}{d_i^{Rx-PoR_2}}\right) \tag{21}$$

where $d_i^{Rx-PoR_2} = \sqrt{\left(x^{Rx} - x_i^{PoR_2}\right)^2 + \left(y^{Rx} - y_i^{PoR_2}\right)^2 + \left(z^{Rx} - z_i^{PoR_2}\right)^2}$ is the distance between the estimated second PoR $\mathbf{PoR}_2^i$ and the receiver $\mathbf{p}^{Rx}$. Similarly, the estimated azimuthal angles of AoA and AoD are estimated as follows respectively:

$$\hat{\theta}_i^{AoD} = \cos^{-1}\left(\frac{y_i^{PoR_1} - y^{Tx}}{d_i^{Tx-PoR_1}}\right) \tag{22}$$

$$\hat{\theta}_i^{AoA} = \cos^{-1}\left(\frac{y_i^{PoR_2} - y^{Rx}}{d_i^{Rx-PoR_2}}\right) \tag{23}$$

Then, we calculate the error between the real and estimated values of azimuthal AoD, elevation AoD, azimuthal AoA and elevation AoA, respectively, as follows:

$$\begin{cases} \epsilon_i^{HAoD} = w2pi\left(\hat{\theta}_i^{AoD} - \theta_i^{AoD}\right) \\ \epsilon_i^{VAoD} = w2pi\left(360 - \hat{\phi}_i^{AoD} - \phi_i^{AoD}\right) \\ \epsilon_i^{HAoA} = w2pi\left(360 - \hat{\theta}_i^{AoA} - \theta_i^{AoA}\right) \\ \epsilon_i^{VAoA} = w2pi\left(360 - \hat{\phi}_i^{AoA} - \phi_i^{AoA}\right) \end{cases} \tag{24}$$

where w2pi is a wrapping function to 180 °.
Then, the estimated first PoR $\mathbf{PoR}_1^i$ is corrected by rotation as follows:

$$\begin{cases} \hat{x}_i^{PoR_1} = \left(x_i^{M_{PoR_1}^{PoR_2}} + \left(x_i^{PoR_1} - x_i^{M_{PoR_1}^{PoR_2}}\right) \times \cos\epsilon_i^{HAoD} - \left(y_i^{PoR_1} - y_i^{M_{PoR_1}^{PoR_2}}\right) \times \sin\epsilon_i^{HAoD}\right) \times \cos\epsilon_i^{VAoD} \\ \hat{y}_i^{PoR_1} = \left(y_i^{M_{PoR_1}^{PoR_2}} + \left(x_i^{PoR_1} - x_i^{M_{PoR_1}^{PoR_2}}\right) \times \sin\epsilon_i^{HAoD} + \left(y_i^{PoR_1} - y_i^{M_{PoR_1}^{PoR_2}}\right) \times \cos\epsilon_i^{HAoD}\right) \times \cos\epsilon_i^{VAoD} \\ \hat{z}_i^{PoR_1} = z_i^{PoR_1} \times \cos\epsilon_i^{VAoD} \end{cases} \tag{25}$$

where $M_{PoR_1^i}^{PoR_2^i} = \left(x_i^{M_{PoR_1}^{PoR_2}}, y_i^{M_{PoR_1}^{PoR_2}}, z_i^{M_{PoR_1}^{PoR_2}}\right)$ is the midpoint between $\mathbf{PoR}_1^i$ and $\mathbf{PoR}_2^i$. Similarly, the estimated second PoR $\mathbf{PoR}_2^i$ is corrected by rotation as follows:

$$\begin{cases} \hat{x}_i^{PoR_2} = \left(x_i^{M_{PoR_1}^{PoR_2}} + \left(x_i^{PoR_2} - x_i^{M_{PoR_1}^{PoR_2}}\right) \times \cos\epsilon_i^{HAoA} - \left(y_i^{PoR_2} - y_i^{M_{PoR_1}^{PoR_2}}\right) \times \sin\epsilon_i^{HAoA}\right) \times \cos\epsilon_i^{VAoD} \\ \hat{y}_i^{PoR_2} = \left(y_i^{M_{PoR_1}^{PoR_2}} + \left(x_i^{PoR_2} - x_i^{M_{PoR_1}^{PoR_2}}\right) \times \sin\epsilon_i^{HAoA} + \left(y_i^{PoR_2} - y_i^{M_{PoR_1}^{PoR_2}}\right) \times \cos\epsilon_i^{HAoA}\right) \times \cos\epsilon_i^{VAoD} \\ \hat{z}_i^{PoR_2} = z_i^{PoR_1} \times \cos\epsilon_i^{VAoD} \end{cases} \tag{26}$$

It is worth mentioning that the reflection coefficient equivalent to the absorption loss can be estimated in the same way as in the single bounce scenario. However, it will correspond to the absorption due to two reflections.

VI. Simulation Results

A. Simulation Environment

We define the position, orientation and antenna characteristics of the transmitter and the receiver placed in a 3D environment with reflecting and blocking obstacles. Scattering, diffraction and vertical propagation are neglected at mmWave. We use image-based ray-tracing method to trace the paths between transmitter and receiver surrounded by obstacles in a 3D environment. The carrier frequency used in $f_c = 60GHz$ with a bandwidth of $BW = 250MHz$. The scenario under test

[3] this assumption is considered here for the ease of derivations. if this information is not available the estimation can still be done at the expense of additional calculation complexity

consists of N transmitters and a receiver. The LoS path does not always exist. Additionally, each path is characterized by a complex amplitude gain and a delay based on environmental properties. The complex amplitude gain of a path is obtained from the transmitter and receiver antenna gain, reflection coefficient and the path attenuation. Antenna gain is related to the radiation patterns. We assume constant complex permittivity for each object.

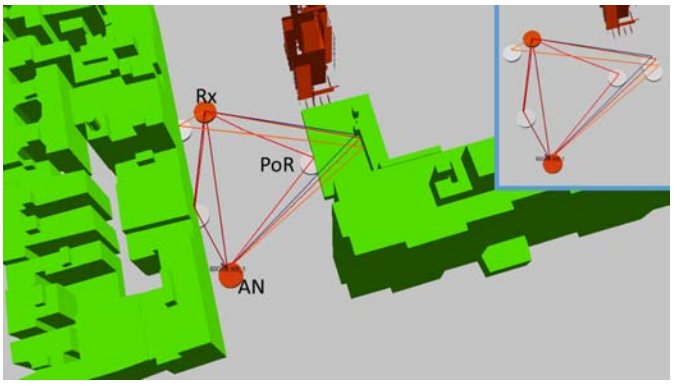

Fig. 4. Vehicular Outdoor Environment, with PoR. The right top corner shows the PoRs without the environment

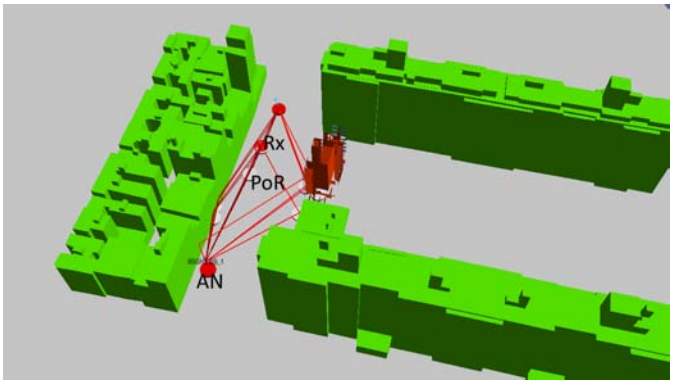

Fig. 5. Another Vehicular Outdoor Environment showing estimated PoR

Reflections are then computed using Fresnels equations as a function of this permittivity and angle-of-incidence. The reflection coefficient is the product of the phase shifts and attenuations. Moreover, path attenuation is modeled by the free-space path loss (FSPL) that defines the gain of the received signal based on the propagating distance d and wavelength λ. The phase shift is represented as a rotation by d/λ in the complex plane. The antennas are assumed to have radiation pattern with 60^o half power beam width (HPBW). In this paper, we consider two particular environments: an outdoor vehicular environment and indoor environment. Each of these environments has been recently of great research interest. Indeed, the framework of 3DLOCMAP can be directly applied in autonomous vehicles to sense and map the obstacles around and in vehicular networks for multiple purposes (detect human crossing the road, sensing the environment, traffic measurement, etc). 3DLOCMAP can be also used for robotics in indoor environment to map objects. In both applications, 3DLOCMAP acts as a radar-like system. All the simulations have been ran using the commercial S_5G Channel Simulator© developed by Siradel.

B. Outdoor Vehicular Environment

The outdoor vehicular environment shown in Fig. 4 consists of a single AN and multiple Rx each considered as a single receiver. Only single and double bounce reflections are considered. As shown in the right top corner of Fig. 4, we are able to estimate the different PoRs including two PoRs for the ray induced by double bounce reflection and two PoRs for the ray induced by single bounce reflection. The result shows accurate detections of PoRs. Similarly, the results in Fig. 5 show the estimation of the PoR for another vehicular outdoor environment. In case of single bounce, the PoR is shown to be estimated accurately. On the other hand, the two PoRs for the double bounce case are estimated with small error. Nevertheless, the achieved information is that the received ray in this case is induced by double reflections. The estimation error is shown in Fig. 6 in terms root mean square error (RMSE) of estimating the PoR (given in terms of its coordinates), distance between the AN and the estimated PoR, and the distance between the AN and the estimated receiver passing through the estimated PoR. The error is shown to increase with the increase of the noise σ^o_{AoA} in AoA measurements. Moreover, the distance between the AN and PoR is estimated with higher error due to the estimation error of the PoR which is due to the error in the AoA. However, the distance traveled by the transmitted ray from the AN to the Rx passing through the PoR is shown to be estimated with higher accuracy since it is based on the ToA measurements and not related to the exact position of the PoR.

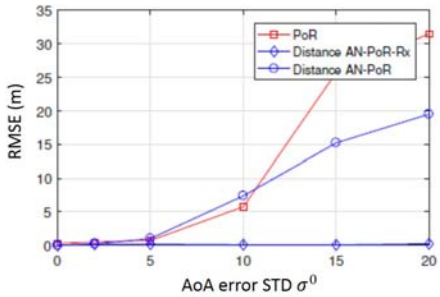

Fig. 6. RMSE measurements for the PoR, Distance AN-PoR-Rx, Distance AN-PoR, Outdoor Vehicular Environment

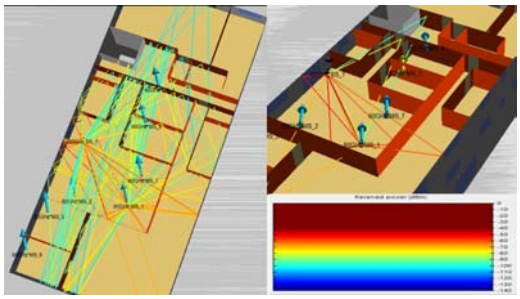

Fig. 7. Indoor Environment

C. Indoor Environment

3DLOCMAP was also implemented in indoor environment. As shown in Fig. 7, the power scale shows the variation of transmitted rays in terms of RSS. The transmitted rays are first filtered based on RSS threshold value γ_{P^r} determined by (2), in which PFA=0.05. Hence, the rays with RSS higher than γ_{P^r}, shown in right top corner in Fig. 7, are used for estimating the Rx and PoR. Similarly, the estimation error shown in Fig. 8 shows higher accuracy in terms of distance traveled from AN to Rx passing through the PoR compared to the estimation of the distance between the AN to PoR that is estimated with additional errors. Nevertheless, indoor environment shows a higher accuracy of estimation compared to outdoor vehicular environment.

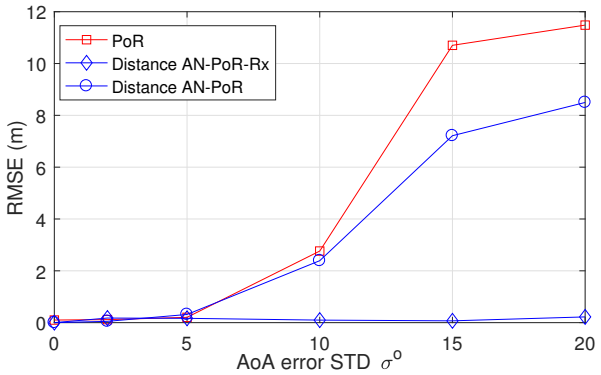

Fig. 8. RMSE measurements for the PoR, Distance AN-PoR-Rx, Distance AN-PoR, Indoor Environment

VII. Conclusion

We presented in this paper 3DLOCMAP and its potential application in vehicular and indoor environments. We proposed in this paper a general framework to estimate the Rx position and estimate the environment through obstacle mapping. The concept of VANs has been introduced from literature to propose a first estimation of the points of reflection. Our work introduced then the concept of virtual receiver highly important in the case of double bounce reflection. The paper results were provided in real scenarios using the commercial 5G Channel Simulator© developed by Siradel. The simulation results have perfectly shown that 3DLOCMAP can perfectly estimate the environment as long as the error in the AoA estimation is less than 5°. Definitely, much work could be achieved in the future. Among others, the localization, detection and classification (object, human, etc) of moving objects will be of order in the future research directions [19].

Acknowledgment

The author Y. Nasser would like to thank and acknowledge the support of 'Safar' Program from the French Embassy in Lebanon for partially funding this work. Authors A. Yassin and Y. Nasser acknowledge the support of Siradel in this work.

References

[1] T. Rappaport et al., *Millimeter Wave Wireless Communications*. Pearson Education, 2014.

[2] Thompson et al., "5G wireless communication systems: prospects and challenges", *IEEE Commun. Mag.*, vol. 52, no. 2, pp. 6264, Feb. 2014.

[3] T. Rappaport et al., "Millimeter wave mobile communications for 5G cellular: It will work!" *IEEE Access*, vol. 1, pp. 335349, 2013.

[4] H. Wymeersch, G. Seco-Granados, G. Destino, D. Dardari and F. Tufvesson, "5G mmWave Positioning for Vehicular Networks," in IEEE Wireless Communications, vol. 24, no. 6, pp. 80-86, Dec. 2017.

[5] J. Choi, V. Va, N. Gonzalez-Prelcic, R. Daniels, C. R. Bhat and R. W. Heath, "Millimeter-Wave Vehicular Communication to Support Massive Automotive Sensing," in IEEE Communications Magazine, vol. 54, no. 12, pp. 160-167, December 2016.

[6] A. Kupper. Location-based services. Wiley, 2005

[7] E. Torkildson, H. Zhang, and U. Madhow, "Channel modeling for millimeter wave MIMO", in *Proc. Information Theory and Applications Workshop*, San Diego, CA, Jan. 2010.

[8] M. K. Samimi and T. S. Rappaport, "Statistical Channel Model with Multi-Frequency and Arbitrary Antenna Beamwidth for Millimeter-Wave Outdoor Communications", *2015 IEEE Globecom Workshops (GC Wkshps)*, San Diego, CA, 2015, pp. 1-7.

[9] L. Subrt, P. Pechac, and S. Zvanovec, "New approach to modeling of diffuse reflection and scattering for millimeter-wave systems in indoor scenarios", *PIERS Online*, vol. 6, 2010.

[10] N. Peinecke, H. Doehler, and B. Korn, "Phong-like lighting for mmWave radar simulation", *in Proc. SPIE*, Cardiff, UK, 2008.

[11] A. Maltsev et al., "Experimental investigations of 60 GHz WLAN systems in office environment", *IEEE J. Sel. Areas Commun.*, vol. 27, no. 8, pp. 14881499, Oct. 2009.

[12] G. R. MacCartney et al., "Path loss models for 5G millimeter wave propagation channels in urban microcells", *in Proc. IEEE GLOBECOM*, Atlanta, GA, Dec. 2013.

[13] Ali Yassin, Youssef Nasser, Mariette Awad, Ahmed Yassin Al-Dubai, "Simultaneous context inference and mapping using mm-Wave for indoor scenarios", In the proceedings of ICC 2017, pp. 1-6, Paris, 2017

[14] M. Bocquet, N. Obeid, C. Loyez, C. Lethien, F. Boukour, N. Rolland, and M. Heddebaut, "Comparison between 60-GHz UWB frequency modulation and UWB impulse-radio location systems", *in Radar Conference*,2008. EuRAD 2008. European, Oct. 2008, pp. 4143.

[15] H. R. Fang, G. P. Cao, E. A. Gharavol, K. Tom, and K. Mouthaan, "60 GHz short range planar RSS localization", *in Proceedings of Asia-Pacific Microwave Conference 2010*, 2010.

[16] D. Dardari, A. Conti, U. Ferner, A. Giorgetti, and M. Z. Win, Ranging With Ultrawide Bandwidth Signals in Multipath Environments, *Proceedings of the IEEE*, vol. 97, no. 2, pp. 404426, Feb. 2009.

[17] A. Conti, M. Guerra, D. Dardari, N. Decarli, and M. Z. Win, Network Experimentation for Cooperative Localization, *IEEE Journal on Selected Areas in Communcations*, vol. 30, no. 2, Feb. 2012.

[18] A. Olivier, G. Bielsa, I. Tejado, M. Zorzi, J. Widmer and P. Casari, "Lightweight Indoor Localization for 60-GHz Millimeter Wave Systems," *2016 13th Annual IEEE International Conference on Sensing, Communication, and Networking (SECON)*, London, 2016, pp. 1-9.

[19] A. Yassin et al., "Recent Advances in Indoor Localization: A Survey on Theoretical Approaches and Applications," *in IEEE Communications Surveys and Tutorials*, vol. 19, no. 2, pp. 1327-1346, Secondquarter 2017.